A new variational approach to deblurring low-resolution images

Wen-Ze Shao, Qi Ge, Li-Qian Wang, Yun-Zhi Lin, Hai-Song Deng

Wen-Ze Shao, Qi Ge, Li-Qian Wang, Yun-Zhi Lin, Hai-Song Deng, "A new variational approach to deblurring low-resolution images," Proc. SPIE 11069, Tenth International Conference on Graphics and Image Processing (ICGIP 2018), 1106919 (6 May 2019); doi: 10.1117/12.2524365

SPIE.

Event: Tenth International Conference on Graphic and Image Processing (ICGIP 2018), 2018, Chengdu, China

A New Variational Approach to Deblurring Low-Resolution Images

Wen-Ze Shao[1,2], Qi Ge[1], Li-Qian Wang[1], Yun-Zhi Lin[3], Hai-Song Deng[4]

[1]College of Telecommunications and Information Engineering, Nanjing University of Posts and Telecommunications (NUPT)
[2]National Engineering Research Center of Communications and Networking, NUPT
[3]School of Automation, Southeast University
[4]School of Science, Nanjing Audit University

ABSTRACT

This paper proposes a new variational model for deblurring low-resolution images, a.k.a. single image nonparametric blind super-resolution. In specific, a type of new adaptive heavy-tailed image priors are presented incorporating both the model discriminativeness and effectiveness of salient edge pursuit for accurate and reliable blur kernel estimation. With the assistance of appropriate non-blind super-resolution approaches, nonparametric blind super-resolution can be cast as a regularized functional minimization problem. An efficient numerical algorithm is derived by harnessing the alternating direction method of multipliers as well as the conjugate gradient method, with which alternatingly iterative estimations for kernel and image are finally implemented in a multi-scale manner. Numerous experiments are conducted along with comparisons made among the proposed approach and two recent state-of-the-art ones, demonstrating that the proposed approach is able to better deal with low-resolution images which are blurred by various possible kernels, e.g., Gaussian-shaped kernels of varying sizes, ellipse-shaped kernels of varying orientations, curvilinear kernels of varying trajectories.

Keywords: Super-resolution, blind deconvolution, camera shake deblurring, normalized sparsity, relative total variation.

1. INTRODUCTION

As a fundamental image restoration task, single-frame super-resolution (SISR) has undergone a rapid development since the pioneering work by Freeman and Pasztor [1] and Baker and Kanade [2]. Several comprehensive surveys [3, 4, 5, 6] present detailed elaborations, comparisons, and also comments on the super-resolution algorithms up to 2013, wherein it is noted clearly that the learning-based strategies manifest more and more potentialities in terms of both accuracy and efficiency, as compared to the more popular variational methods in the scenario of multi-frame super-resolution. The basic idea of learning-based SISR approaches is to learn a single or multiple mappings between the low-res (LR) and high-res (HR) domains by harnessing a large set of training image pairs, where every HR training image is blurred by a supposed bicubic or Gaussian kernel. The representative learning-based single image super-resolution (SISR) approaches essentially originate from three kinds of machine learning methodologies, i.e., manifold learning, sparse learning, and deep learning, based on which four types of SISR algorithms are summarized as follows: *neighborhood embedding* [7, 8], *coupled dictionary learning* [9, 10], *locally-linear regression* [11, 12], and *convolutional neural networks* [13, 14].

Though SISR has earned intensive attention in the past two decades, a careful inspection reveals that there exists a common assumption in the current literature, namely, the high-res image is blurred by a supposed bicubic or Gaussian blur kernel with a known standard deviation. And actually, most of existing learning-based approaches use the bicubic low-pass filter (implemented via MATLAB's default function *imresize*) to generate the LR-HR training pairs. We note that apparently the parametric assumption on the form of blur kernels does not hold in most practical applications, as in real LR imaging an HR image would be generally undergone a complicated blur process, e.g., Gaussian-shaped kernels of varying sizes, ellipse-shaped kernels of varying orientations, curvilinear kernels of varying trajectories. According to literature review, only few works have addressed estimating an accurate blur kernel within the scenario of SISR. Among few such contributions, a parametric model is usually assumed and the Gaussian is a common choice. However, as the

Tenth International Conference on Graphics and Image Processing (ICGIP 2018), edited by Chunming Li, Hui Yu, Zhigeng Pan, Yifei Pu, Proc. of SPIE Vol. 11069, 1106919
© 2019 SPIE · CCC code: 0277-786X/19/$18 · doi: 10.1117/12.2524365

assumption does not coincide with the actual blur model. To the best of our knowledge, the first daring attempt towards nonparametric blur kernel estimation for single image SR is made in [15] and its problem solution also applies to blind image deblurring. However, it restricts its treatment to single peak blur kernels and does not originate from a rigorous optimization principle but relies on empirical detection and prediction of step edges as important clues to blur kernel estimation. A second noteworthy work for nonparametric blind SR is the one by Michaeli and Irani [16] whose essential idea is to harness the recurrence property of natural image patches across different scales. It should be noted that the performance of this approach relies heavily on the searched nearest neighbors to the query patches in the input blurred, low-res image. In the meanwhile, as claimed in [17] the nonparametric blind SR approach [16] cannot be naively applicable to blind image deblurring. Taking into account the similarity between blind deconvolution and blind SR in terms of nonparametric blur kernel estimation, the first author of the present paper and his collaborator recently propose to formulate both blind problems in a common modeling viewpoint [18, 19], i.e., bi-L_0-L_2-norm regularization. Although the endeavor being made in [18] is preliminary, it brings us an enlightenment that the gap between two blind restoration problems can be narrowed to a certain degree.

In this paper, we build on our preliminary work in [18] while taking a step further. Specifically, we develop a novel ADMM method for nonparametric blind SR by proposing a type of L_α-norm based adaptive heavy-tailed image priors, to some extent, which can be expressed and understood as a generalized integration of the previous normalized sparsity measure and relative total variation. Combining the adaptive priors and the convolutional consistency constraint (CCC) as advocated in [18], an intermediate high-res image of higher quality becomes possible and hence more accurate blur kernel estimation can be achieved for the nonparametric blind SR task. As for minimization of the resulting functional, an ADMM-based iterative algorithm is derived for estimating the intermediate high-res image and nonparametric blur kernel alternatingly, during which the conjugate gradient algorithm is exploited for running efficiency. A great many experiments are performed on both synthetic and real-world blurred low-res images, demonstrating the comparative or even superior performance of the proposed method convincingly. An empirical study is also made towards appropriate choice of existing SISR algorithms for the convolutional consistency constraint, and the candidates are from the four categories of learning-based SISR methods mentioned above, considering their inbred advantages in terms of both accuracy and efficiency. It is not surprised that the empirical observation conforms to that in [18], i.e., ANR (anchored neighborhood regression) [11] is shown a more robust engine for our purpose than other candidates including the those deep learning-based methodology.

2. PROPOSED SPATIALLY ADAPTIVE HEAVY-TAILED PRIORS

Considering both the modeling effectiveness and computational efficiency, a type of new heavy-tailed image priors are proposed to regularize the blur kernel estimation process, expressed as

$$p(u) \propto \prod_{p\in\Omega} exp\left\{-\gamma_{x,p}(u)\cdot\left|\partial_x u_p\right|^\alpha - \gamma_{y,p}(u)\cdot\left|\partial_y u_p\right|^\alpha\right\} \tag{1}$$

where $p \in \Omega$ denotes a pixel index in the region Ω, $0 < \alpha \le 1$ amounts to imposing the L_α-norm based regularization on images, $\gamma_{x,p}(u)$ and $\gamma_{y,p}(u)$ are the spatially adaptive weights defined for each image pixel in the horizontal and vertical directions, embodying one of our core contributions in this paper. On one hand, $p(u)$ as in (1) is expected potentially discriminative so as to ensure the success of blur kernel estimation, i.e., sharp high-res images should be favored rather than their blurred counterparts and then the delta kernel can be avoided. On the other hand, $p(u)$ as in (1) is expected ease of fast iterative computations of the nonparametric blur kernel and itermediate sharp image. Hence, in order to boost the discriminativeness of normalized sparsity measure and more importantly its real performance in kernel estimation, in the proposed heavy-tailed priors the spatially adaptive weight $\gamma_o(u_p)$, $o \in \{x, y\}$ is presented as

$$\gamma_o(u_p) = \frac{1-\varpi}{G_o(u)+\varepsilon} + \frac{\varpi}{L_o(p)+\varepsilon} \tag{2}$$

where $\varpi \in (0, 1)$, ε is a small positive value to avoid division by zero, and $G_o(u)$, $L_o(p)$ are defined, respectively, as

$$G_o(u) = \sqrt{\sum_{p\in\Omega(u)}\left|\partial_o u_p\right|^2} = \left\|\partial_o u\right\|_2 \tag{3}$$

$$L_o(p) = \left|\sum_{q\in N(p)} \phi_{p,q}\cdot\partial_o u_q\right| \tag{4}$$

where $\Omega(u)$ denotes the entire image field, $\boldsymbol{N}(p)$ is a rectangular region centered at the pixel p, and $\phi_{p,q}$ is defined according to the spatial affinity as a distance function of Gaussianity, i.e.,

$$\phi_{p,q} \propto \exp\left(-\frac{(x_p - x_q)^2 + (y_p - y_q)^2}{2\sigma^2}\right) \tag{5}$$

where σ is a spatial scale to be specified in implementation.

Let us dive into (1) and (2) for more details on the modeling properties of the proposed heavy-tailed priors. To make the analysis clearer, we study the negative logarithm of $p(u)$ which is denoted as

$$R(\partial u) \triangleq -\log p(u) = \sum_{p\in\Omega} \gamma_x(u_p) \cdot \left|\partial_x u_p\right|^{\alpha} + \gamma_y(u_p) \cdot \left|\partial_y u_p\right|^{\alpha} \tag{6}$$

That is, $R(\partial u)$ can be viewed as the deterministic regularization on the image u. We note that the terms $G_o(u)$ and $L_o(p)$ were previously exploited in [20] and [21], respectively. Particularly, when α is set as 1, the proposed regualrization (6) will degenerate to the normalized sparsity measure upon ϖ specified as 0, while to the relative total variation (RTV) upon ϖ specified as 1. Hence, (6) is actually a gradient-based composite model specifically designed for blur kernel estimation. We should also note that RTV is originally proposed for structure-preserving image filtering and manipulation, whose value in a window just containing textures is statistically found smaller than that in a window also including structural edges. To the best of our knowledge, none of existing works exploits RTV as a regualrization term for nonparametric blind SISR. Therefore, it can be intuitively concluded that the core idea of the proposed prior is to amend the generalized normalized sparsity measure $\sum_{p\in\Omega} |\partial_x u_p|^{\alpha} / G_x(u) + \sum_p |\partial_y u_p|^{\alpha} / G_y(u)$ by the additional generalized RTV $\sum_{p\in\Omega} |\partial_x u_p|^{\alpha} / L_x(p) + \sum_p |\partial_y u_p|^{\alpha} / L_y(p)$, in the sense that a higher quality intermediate sharp image with interfering details/textures removed is to be produced as a core assurance to the kernel estimation precision. Experimental results along with empirical anaysis are to be provided in Section 4 for better understanding the coupling superiority of the proposed model.

3. VARIATIONAL BLIND SUPER-RESOLUTION: FORMULATION AND ALGORITHM

Let $\mathbf{g}$ be the vector form of the low-res image o with size $N_1 \times N_2$, and $\mathbf{u}$ the vector form of the corresponding high-res image u with size $sN_1 \times sN_2$, where $s > 1$ is an upsampling factor. Then, the relation between $\mathbf{g}$ and $\mathbf{u}$ can be expressed into two equivalent matrix-vector forms

$$\mathbf{g} = \mathbf{DKu} + \mathbf{n} \quad \text{or} \quad \mathbf{g} = \mathbf{DUk} + \mathbf{n} \tag{7}$$

where $\mathbf{U}$ and $\mathbf{K}$ are assumed two BCCB (block-circulant with circulant blocks) convolution matrices corresponding to the vectorized high-res image $\mathbf{u}$ and blur kernel $\mathbf{k}$, and $\mathbf{D}$ denotes a down-sampling matrix, and $\mathbf{n}$ is the possible zero-mean white Gaussian noise. Note that, in implementation image boundaries are smoothed in order to supress the border artifacts, just the same as in [18]. Then, our task is to infer $\mathbf{u}$ and $\mathbf{k}$ provided only the low-res image $\mathbf{g}$ and the up-sampling factor s. As emphasized above, our adaptive heavy-tailed priors are unnatural since faint details/textures are to be smeared out among the blur kernel estimation. Hence the nonparametric blind SR task is divided into wo independent stages, i.e., (*a*) alternatingly estimating the nonparametric blur kernel $\mathbf{k}$ and the intermediate high-res image $\mathbf{u}$ using the derived numerical scheme to be specified in the following; (b) estimating the final sharp high-res image with a state-of-the-art non-blind SR method.

As demonstrated in [18], the accuracy of blur kernel estimation for the blind SR task is also affected by the jagging artifacts along the salient edge structures except for the interfering details/ textures. Then, the complete formulation for alternatingly estimating the nonparametric blur kernel $\mathbf{k}$ and the intermediate high-res image $\mathbf{u}$ can be given as

$$\hat{\mathbf{u}}, \hat{\mathbf{k}} = \arg\min_{\mathbf{u},\mathbf{k}} \frac{\eta}{2}\left\|\mathbf{g} - \mathbf{DKu}\right\|_2^2 + \lambda \boldsymbol{R}(\nabla \mathbf{u}) + \frac{\beta}{2}\left\| \mathbf{u} - \mathbf{K}\,\mathbf{u}\right\|_2^2 + \left\|\mathbf{k}\right\|_{0.5}^{0.5} \tag{8}$$

where η, λ, β are positive tuning parameters, $\boldsymbol{R}(\nabla \mathbf{u})$ is the vectorized form of the regularization term $R(\partial u)$, $\nabla \mathbf{u} \triangleq [\nabla_x \mathbf{u}; \nabla_y \mathbf{u}]$, where $\nabla_x \mathbf{u} = [\partial_x \mathbf{u}_1, \partial_x \mathbf{u}_2, ..., \partial_x \mathbf{u}_{sN_1 \times sN_2}]^T$, $\nabla_y \mathbf{u} = [\partial_y \mathbf{u}_1, \partial_y \mathbf{u}_2, ..., \partial_y \mathbf{u}_{sN_1 \times sN_2}]^T$, and ∇_x, ∇_y are the convolutional matrices corresponding to the partial derivative operators ∂_x, ∂_y, and the last term is the $L_{0.5}$-norm based regularization imposed on the blur kernel $\mathbf{k}$ which is an empirical choice just similar to the conventional practice made in

the blind deblurring community. To be noted that $\boldsymbol{R}(\nabla \mathbf{u})$ is responsible for pursing the accurate salient edges as core clues to kernel estimation, which, however, cannot be achieved without the third term $\|\breve{\mathbf{u}} - \mathbf{K}\mathbf{u}\|_2^2$ due to the very possible jagging artifacts emerged in the naïve upsampling process, which is named the convolutional consistency constraint (CCC) in our previous blind SR work [18]. The rationale in the CCC is that using an appropriate learning-based SR model which is generated with a bicubic kernel, the super-resolved blurred image $\breve{\mathbf{u}}$ approximately satisfies the relation $\mathbf{K}\mathbf{u} \approx \breve{\mathbf{u}}$. To gain the idea of the proposed formulation (8) intuitively, four representative learning-based non-blind SR models are experimented, including: *neighborhood embedding* (NE) [8], *joint sparse coding* (JSC) [10], *anchored neighborhood regression* (ANR) [11], and *deep convolutional network* (DCN) [13], in consideration of their inbred advantages in terms of both accuracy and efficiency.

In Figure 1, a low-res version of a high-res image "bird" is provided, which is blurred by a 19×19 Gaussian kernel with *standard deviation* 2.5 and down-sampled by a factor 3. Note that in estimation the proposed approach is blind to the blur kernel shape, size, and standard deviation, and hence we just assume the kernel size as 31×31 which is normally large enough for the blind SR problem. The true blur kernel is also presented in the first column of **Figure 1** accompanied with the the original high-res image "bird". The remaining columns provide the SR results by those non-blind learning-based approaches as above and our proposed blind method boosted by each of them respectively. For example, the second column shows two super-resolved images via ANR [11] and our method boosted by ANR as formulated in (8), simply denoted as Blind-ANR for convenience of description. It is seen that the outputs of four non-blind SR methods [11, 13, 10, 8] are all blurry images while our blind approach is able to generate visually clear images. The metric PSNR, i.e., peak signal-to-noise ratio, is used to evaluate those non-blind and blind super-resolved images quantitatively. We also use the metric SSD, i.e., sum of squared difference [22], to quantify the error between the estimated blur kernel and its counterpart ground truth. It is apparent that the proposed Blind-ANR has achieved the best performance in terms of the image PSNR value in this example whose estimated blur kernel most resembles the ground truth in terms of the kernel SSD value.

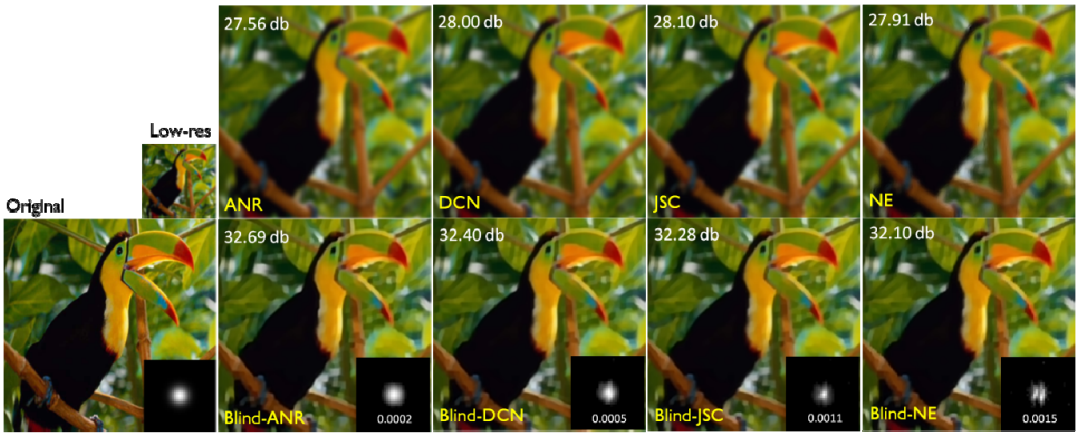

Figure 1. An illustrative example of the proposed approach to nonparametric blind SR harnessing advanced learning-based methods including: ANR [11], DCN [13], JSC [10], NE [8]. First row: low-res image $\mathbf{g}$ and non-blind super-resolved images $\breve{\mathbf{u}}$; Second row: original high-res image $\mathbf{u}$ and blind super-resolved images accompanied by the true and estimated blur kernels. The image PSNR and kernel SSD are calculated and provided for quantitative evaluation. The proposed Blind-ANR has achieved the best performance in terms of the image PSNR value in this example whose estimated blur kernel most resembles the ground truth in terms of the kernel SSD value.

Furthermore, we provide another illustrative example in Figure 2 where the high-res image "alphabet table" is blurred by a nonparametric motion blur kernel with size 11×11 and down-sampled by a factor 2. We see that the proposed Blind-ANR outperforms Blind-DCN, Blind-JSC and Blind-NE by a large margin in terms of the image PSNR in this example, and that the four blind approaches have also overwhelmed their corresponding non-blind counterparts. In the meantime, it is conjectured from this example that the kernel metric SSD may be not absolutely fair for evaluating the performance of nonparametric blind SR approaches. In brief, above two examples demonstrate well the feasibility and effectiveness of our adaptive heavy-tailed image priors, and validate that the non-blind SR method ANR [11] can be

used as a more robust engine for our framework compared against several other candidates including the advanced deep learning-based methodology [13] which conforms to the empirical finding in [18].

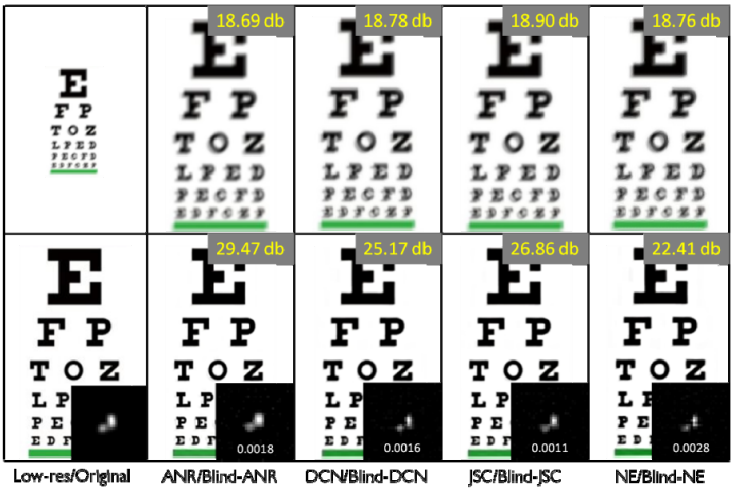

Figure 2. An illustrative example of the proposed approach to nonparametric blind SR harnessing advanced learning-based methods including: ANR [11], DCN [13], JSC [10], NE [8]. First row: low-res image $\mathbf{g}$ and non-blind super-resolved images $\breve{\mathbf{u}}$; Second row: original high-res image $\mathbf{u}$ and blind super-resolved images accompanied by the true and estimated blur kernels. The image PSNR and kernel SSD are calculated and provided for quantitative evaluation. The proposed Blind-ANR has achieved the best performance in terms of the PSNR value in this example, however whose estimated blur kernel does not most resemble the ground truth in terms of the SSD value. Blind super-resolved images can be observed on the computer screen for better visual comparison.

In this paper, we do not attempt to provide a rigorous theoretical analysis on the existence of a global minimizer of (8) or further make a claim regarding the convergence of the proposed numerical scheme. Instead, our concentration is on a practical numerical algorithm considering the blind nature of our problem. In the normal, the problem can be directly expressed as alternating minimization of (8), i.e., provided the $(i\text{-}1)^{th}$ iterative solutions of $\mathbf{u}^{(i-1)}$ and $\mathbf{k}^{(i-1)}$, $\mathbf{u}^{(i)}$ and $\mathbf{k}^{(i)}$ can be obtained by respectively solving (9) and (10) as follows

$$\mathbf{u}^{(i)} = \arg\min_{\mathbf{u}} \frac{\eta}{2}\left\|\mathbf{g} - \mathbf{D}\mathbf{K}^{(i-1)}\mathbf{u}\right\|_2^2 + \lambda \boldsymbol{R}\left(\mathbf{u}^{(i-1)}, \nabla\mathbf{u}\right) + \frac{\beta}{2}\left\|\breve{\mathbf{u}} - \mathbf{K}^{(i-1)}\mathbf{u}\right\|_2^2 \tag{9}$$

$$\mathbf{k}^{(i)} = \arg\min_{\mathbf{k}} \frac{\eta}{2}\left\|\mathbf{g} - \mathbf{D}\mathbf{U}^{(i)}\mathbf{k}\right\|_2^2 + \frac{\beta}{2}\left\|\breve{\mathbf{u}} - \mathbf{U}^{(i)}\mathbf{k}\right\|_2^2 + \left\|\mathbf{k}\right\|_{0.5}^{0.5} \tag{10}$$

where $1 \le i \le I = 10$, $\mathbf{K}^{(i-1)}$ and $\mathbf{U}^{(i)}$ are the convolution matrices corresponding to the estimates $\mathbf{k}^{(i-1)}$ and $\mathbf{u}^{(i)}$, and $\boldsymbol{R}\left(\mathbf{u}^{(i-1)}, \nabla\mathbf{u}\right)$ is an iterative version of $\boldsymbol{R}\left(\nabla\mathbf{u}\right)$. We should note that our empirical experimentation suggests that the kernel update step can be better performed as implemented in the image derivative domain. Note that this has been also validated in [18] and several blind image deburring works such as [19, 20]. Therefore, (10) is modified as

$$\mathbf{k}^{(i)} = \arg\min_{\mathbf{k}} \sum_{o\in\{x,y\}} \left\{\frac{\eta}{2}\left\|\mathbf{g}_o - \mathbf{D}\mathbf{U}_o^{(i)}\mathbf{k}\right\|_2^2 + \frac{\beta}{2}\left\|\breve{\mathbf{u}}_o - \mathbf{U}_o^{(i)}\mathbf{k}\right\|_2^2\right\} + \left\|\mathbf{k}\right\|_{0.5}^{0.5} \tag{11}$$

where $\mathbf{g}_o = \nabla_o\mathbf{g}$, $\breve{\mathbf{u}}_o = \nabla_o\breve{\mathbf{u}}$, $\mathbf{U}_o^{(i)}$ denotes the convolutional matrix of the image gradient $\mathbf{u}_o^{(i)} = \nabla_o\mathbf{u}^{(i)}$. Besides, $\mathbf{k}^{(i)}$ should be projected onto the constraint set $\mathcal{C} = \{\mathbf{k} \ge 0,\ \|\mathbf{k}\|_1 = 1\}$ because a blur kernel is non-negative and normalized.

As minimizing the resulted functionals (9) and (11), an ADMM-based iterative algorithm is derived for estimating the intermediate high-res image and nonparametric blur kernel alternatingly, during which the conjugate gradient algorithm is exploited for running efficiency. Meanwhle, following the regular practice in blind image deconvolution, a multi-scale strategy is harnessed for the final algorithm so as to make our method applicable to large-scale blur kernel estimation and also avoid stuck into poor local minima when solving (9) and (11). The pseduo code of the final algorithm is summarized

as **Algorithm 1**. In each scale, the low-res image $\mathbf{g}$ and the super-resolved blurry image $\breve{\mathbf{u}}$ generated by ANR are 2 times down-sampled successively as inputs to (9) and (11). In the finest scale the inputs are the original $\mathbf{g}$ and $\breve{\mathbf{u}}$ themselves. The initialized image for each scale is set as the down-sampled $\breve{\mathbf{u}}$, and the initialized kernel is set as the bicubic up-sampled blur kernel estimated in the coarser scale (in the coarsest scale the initial kernel is simply set as the Dirac pulse). Furthermore, inspired by the blind deblurring literature a continuation scheme on the parameters η, β is also applied for better performation. It is not hard to find that the main computational cost of the proposed approach is on the iterative estimates of $\mathbf{u}_l^{(i-1)}$, $\mathbf{k}_j^{(i-1)}$, which have been based on the CG algorithm due to the involved down-sampling operator in the low-res imaging model. With the estimated blur-kernel $\hat{\mathbf{k}}$, the final high-res image is generated using the TV-based SR method [23].

Algorithm 1. Blur kernel estimation for nonparametric blind SR

input : low-res image $\mathbf{g}$, up-sampling factor r, super-resolved image $\breve{\mathbf{u}}$, η, λ, β, ϖ.
multi - scale processing : $\{\mathbf{g}_s\}$, $\{\breve{\mathbf{u}}_s\}$, $s \le 4$.
initializer : $i \leftarrow 0$, $\mathbf{k}^{(0)} \leftarrow$ Dirac pulse, $\mathbf{u}^{(0)} \leftarrow \breve{\mathbf{u}}_1$.
while $s \le 4$ **do**
    while $i \le 10$ **do**
        set $\mathbf{u}_0^{(i-1)} \leftarrow \mathbf{u}^{(i-1)}, \mathbf{r}_0^{(i-1)} \leftarrow \mathbf{0}$.
        solve (8) for $\mathbf{u}^{(i)}$ with 10 iterations of iterative estimates of $\mathbf{u}_l^{(i-1)}, \mathbf{r}_l^{(i-1)}$.
        set $\mathbf{k}_0^{(i-1)} \leftarrow \mathbf{k}^{(i-1)}, \mathbf{z}_0^{(i-1)} \leftarrow \mathbf{0}$.
        solve (10) for $\mathbf{k}^{(i)}$ with 10 iterations of iterative estimates of $\mathbf{k}_j^{(i-1)}, \mathbf{z}_j^{(i-1)}$.
        set $\eta \leftarrow 1.25 \cdot \eta$, $\beta \leftarrow 1.25 \cdot \beta$.
    end while
    set $i \leftarrow 0$.
    set $\mathbf{k}^{(0)} \leftarrow$ bicubic up-sampled kernel of scale s with projection onto the set $\mathcal{C}$.
    set $s \leftarrow s + 1$.
    set $\mathbf{u}^{(0)} \leftarrow \breve{\mathbf{u}}_s$.
end while
output : blur kernel $\hat{\mathbf{k}}$.
non - blind SR : super-resolve the final high-res image using the TV-based SR method [23] given the estimated kernel $\hat{\mathbf{k}}$.

4. EXPERIMENTAL RESULTS

Considering the fact that the work in [16] loses its stability for large kernels[1], we restrict the size of unknown kernels to 19×19 universally across all the experiments in the following. Besides, both the bi-L_0-L_2-norm based blind SR method [18] and our approach in **Algorithm 1** choose ANR [11] for obtaining the non-blind super-resolved image $\breve{\mathbf{u}}$. To quantify the performance of different blur kernel estimation methods, values of PSNR and SSIM corresponding to each of the final super-resolved SR image are computed. As for the parameter settings of the proposed method, η, λ, β are specified to be 0.01, 0.25, and 100, respectively. Another parameter is the balance coefficient ϖ in the proposed heavy-tailed image prior (1), which is found matter a lot to the estimation accuracy, and in this paper it is fixed to be 0.1. For the sake of description clarity, the work in [16] is named of Patch Recurrency and that in [18] is named of bi-L_0-L_2-norm.

[1] In [16] blur-kernels are typically solved with size 9×9, 11×11 or 13×13 for various blind SR problems.

4.1 Super-resolving synthetic blurred low-res images

In this group of experiments, each of the thirty test images from the Berkeley Segmentation Dataset as shown in Figure 3 is blurred by a 11×11 Gaussian kernel with *standard variation* 2.5, down-sampled with a factor 3, and degraded by a zero-mean white Gaussian noise with noise level 1. The average blur kernel SSD, image PSNR, and image SSIM corresponding to each of compared methods are provided in Table 1. We see that in this scenario the proposed approach has achieved comparable performance to [18] in terms of either kernel SSD or image SSIM and PSNR. It is also noticed that the Patch Recurrency method by Michaeli and Irani [16] can not generate state-of-the-art results in spite of their fresh ideas. For visual perception, the super-resolved images are provided in Figure 4 and 5 corresponding respectively to images with No. 10 and 13, where the intermediate images produced by the proposed method are also shown. Clearly, it is observed that the estimated blur kernels by [16] and the proposed method are more accurate than those by [16].

Figure 3. Thirty test images from the Berkeley Segmentation Dataset for nonparametric blind SR in the scenario of Gaussian blur.

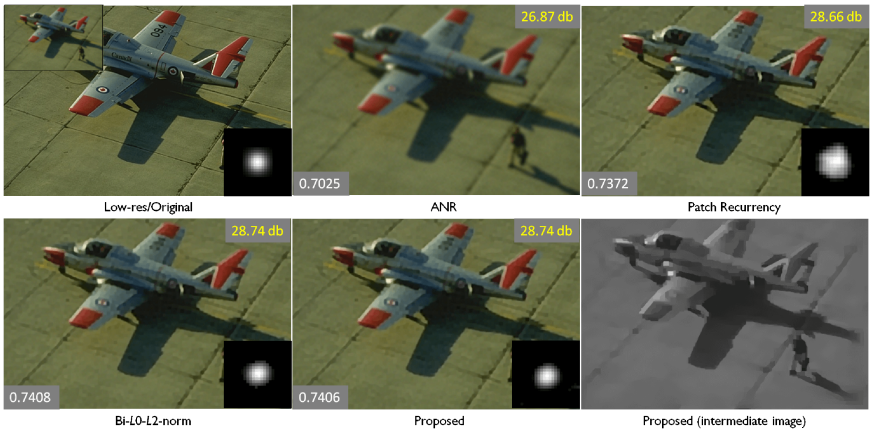

Figure 4. Super-resolved images along with values of SSIM and PSNR by ANR [11] (0.7025, 26.87 dB), Patch Recurrency [16] (0.7372, 28.66 dB), bi-L_0-L_2-norm [18] (0.7408, 28.74 dB), and our approach (0.7406, 28.74 dB).

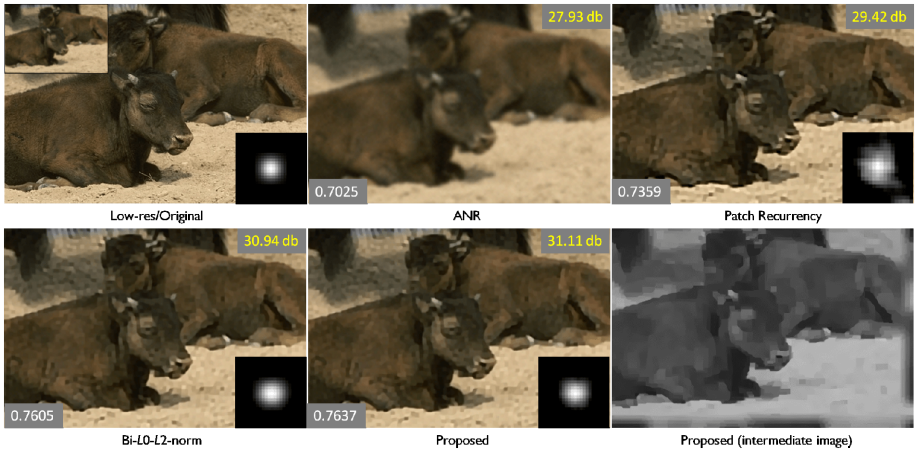

Figure 5. Super-resolved images along with values of SSIM and PSNR by ANR [11] (0.7025, 27.93 dB), Patch Recurrency [16] (0.7359, 29.42 dB), bi-L_0-L_2-norm [18] (0.7605, 30.94 dB), and our approach (0.7637, 31.11 dB).

Table 1. Nonparametric blind SR in the scenario of Gaussian blur with average kernel SSD, image SSIM, and image PSNR provided corresponding to Patch Recurrency [16], bi-L_0-L_2-norm [18], and the proposed approach (Ours)

Image No.	[16]			[18]			Ours		
	SSD	SSIM	PSNR	SSD	SSIM	PSNR	SSD	SSIM	PSNR
1	0.0020	0.9327	33.62	0.0006	0.9521	36.04	0.0004	0.9537	36.20
2	0.0017	0.7640	27.02	0.0003	0.8122	29.17	0.0005	0.8104	29.12
3	0.0020	0.6178	26.26	0.0003	0.6587	27.29	0.0007	0.6550	27.20
4	0.0034	0.8174	31.02	0.0004	0.8558	33.79	0.0003	0.8571	33.78
5	0.0030	0.6273	24.92	0.0001	0.6975	27.60	0.0002	0.6975	27.68
6	0.0062	0.6116	23.89	0.0007	0.6987	26.68	0.0002	0.6975	26.63
7	0.0039	0.6449	24.36	0.0001	0.7023	26.71	0.0004	0.6994	26.63
8	0.0062	0.7257	23.42	0.0001	0.7960	25.45	0.0004	0.7886	25.22
9	0.0097	0.3411	17.75	0.0002	0.5351	21.26	0.0004	0.5283	21.20
10	0.0005	0.7372	28.66	0.0003	0.7408	28.74	0.0002	0.7406	28.74
11	0.0044	0.4915	24.66	0.0002	0.5531	27.20	0.0003	0.5539	27.21
12	0.0061	0.5684	23.02	0.0002	0.6567	26.26	0.0002	0.6570	26.35
13	0.0014	0.7359	29.42	0.0004	0.7605	30.94	0.0002	0.7637	31.11
14	0.0014	0.4221	23.76	0.0001	0.4364	24.29	0.0003	0.4347	24.27
15	0.0027	0.7490	28.06	0.0003	0.7819	29.51	0.0001	0.7840	29.63
16	0.0016	0.8671	27.47	0.0007	0.9060	29.77	0.0002	0.9050	29.70
17	0.0016	0.7680	28.92	0.0003	0.7872	29.80	0.0003	0.7874	29.71
18	0.0033	0.8550	28.47	0.0001	0.9105	34.27	0.0001	0.9102	34.33
19	0.0036	0.5810	24.46	0.0003	0.6542	28.24	0.0002	0.6551	28.23
20	0.0026	0.4343	21.78	0.0001	0.4745	22.62	0.0006	0.4668	22.57
21	0.0048	0.5150	20.65	0.0003	0.5347	21.01	0.0005	0.5336	21.00
22	0.0032	0.7039	24.88	0.0001	0.7266	25.60	0.0003	0.7226	25.49
23	0.0044	0.4607	22.83	0.0001	0.5324	24.99	0.0003	0.5304	24.96
24	0.0014	0.6368	26.60	0.0001	0.6607	27.54	0.0002	0.6588	27.52
25	0.0084	0.6583	26.87	0.0002	0.7300	29.73	0.0003	0.7300	29.70
26	0.0041	0.4485	24.47	0.0001	0.5267	27.39	0.0003	0.5236	27.33
27	0.0015	0.5617	24.94	0.0017	0.5853	24.88	0.0002	0.5848	25.22
28	0.0034	0.5961	27.28	0.0001	0.6560	28.86	0.0002	0.6548	28.85
29	0.0039	0.6168	24.35	0.0001	0.6934	26.13	0.0003	0.6920	26.07
30	0.0036	0.5769	23.71	0.0002	0.6638	25.83	0.0003	0.6610	25.79
Average	**0.0035**	**0.6356**	**25.58**	**0.0003**	**0.6893**	**27.59**	**0.0003**	**0.6879**	**27.58**

4.2 Super-resolving real-world blurred low-res images

In order to validate the robustness of the proposed method to the parameter settings, they are specified exactly the same as those in the sythetic experiments in subsection 4.1. In addition, the size of blur kernels for each method is still set as 19×19. We also suggest that one should observe the super-resolved images provided below on the computer screen for better qualitiative comparison among different methods.

In Figure 6, another old picture is also 2 times super-resolved with different methods. We see that the non-blind approach ANR [11] produces a very blurry image, reflecting the necessity of single image blind SR techniques. We also observe that both the proposed approach and bi-L_0-L_2-norm [18] generate visually pleasant high-res images and also reasonable blur kernels from which it is conjectured that the low-res image had undergone a camera shake blur. Meanwhile, it is seen that the super-resolved image by Patch Recurrency method [16] is very similar to those by another two methods, but a careful inspection tells that the true blur kernel should not have a support as large as that estimated by [16]. In Figure 7, an iphone picture is 3 times super-resolved, and the result image by ANR [11] is apparently much blur as compared against the results by the three non-parametric blind methods. Observing the estimated blur kernels we see that the orientation of the kernel by bi-L_0-L_2-norm [18] resembles a lot that of the kernel by our method while our kernel support is more accurate because one may insepct that our super-resolved image is visually clearer; in the meanwhile it is noticed the support of the kernel by Patch Recurrency [16] resembles that of the kernel by our approach but our kernel orientiation seems more accurate because of the slightly better visual perception on our super-resolved image.

Figure 6. Blind super-resolution (2 times) by ANR [11], Patch Recurrency [16], bi-L_0-L_2-norm [18], and the proposed approach.

Figure 7. Blind super-resolution (3 times) by ANR [11], Patch Recurrency [16], bi-L_0-L_2-norm [18], and the proposed approach.

5. CONCLUSION

Single image nonparametric blind super-resolution is a fundamental image restoration problem yet having been largely ignored in the past decades among the computational photography and computer vision communities. This paper is majorly motivated by one of our previous works [18], while takes a step further and presents a type of adaptive heavy-tailed image priors, which result in a new regularized formulation for nonparametric blind super-resolution. To some extent, the new prior may be expressed and understood as a generalized integration of the previous normalized sparsity

measure and relative total variation. Harnessing the prior, a higher quality intermediate high-res image becomes possible and therefore more accurate blur kernel estimation can be accomplished. A great many experiments are performed on both synthetic and real-world blurred low-res images, demonstrating the comparative or even superior performance of the proposed algorithm convincingly.

6. ACKNOWLEDGEMENTS

The study is supported in part by the Natural Science Foundation (NSF) of China (61771250, 61402239, 61602257, 61502244, 11671004), the NSF of Jiangsu Province (BK20160904, BK20150859), the NSF for Jiangsu Institutions (16KJB520035), and the Open Fund of National Engineering Research Center of Communications and Networking (Nanjing University of Posts and Telecommunications, TXKY17008).

REFERENCES

[1] W.T. Freeman, E.C. Pasztor, "Learning to estimate scenes from images," *Advances in Neural Information Processing Systems (NIPS)*, pp. 775-781, (1999)

[2] S. Baker, T. Kanade, "Hallucinating faces," *Proc. IEEE Conf. Automatic Face and Gesture Recognition*, pp. 83-88, (2000)

[3] P. Milanfar, "Super-resolution Imaging," CRC Press, (2011)

[4] J. Tian, K.-K. Ma, "A survey on super-resolution imaging," *Signal, Image and Video Processing*, 5(3): 329-342, (2011)

[5] K. Nasrollahi, T.B. Moeslund, "Super-resolution: a comprehensive survey," *Machine Vision and Applications*, 25: 1423-1468, (2014)

[6] C.-Y. Yang, C. Ma, M.-H. Yang, "Single-image super-resolution: A benchmark," *Proc. European Conf. Computer Vision (ECCV)*, pp. 372-386, (2014)

[7] M. Bevilacqua, A. Roumy, C. Guillemot, and M.-L. A. Morel, "Low-complexity single-Image super-resolution based on nonnegative neighbor embedding," *British Mach. Vis. Conf.*, pp. 1-10, (2012)

[8] H. Chang, D.-Y. Yeung, and Y. Xiong, "Super-resolution through neighbor embedding," *IEEE Int. Conf. Comput. Vis. Pattern Recognit. (CVPR)*, pp. 275-282, (2004)

[9] J. Yang, J. Wright, T. S. Huang, and Y. Ma, "Image super-resolution via sparse representation," *IEEE Trans. Image Process.*, vol. 19, no. 11, pp. 2861-2873, (2010)

[10] R. Zeyde, M. Elad, and M. Protter, "On single image scale-up using sparse representation," Int. Conf. Curves & Surfaces, vol. 6920, pp. 711-730, (2010)

[11] R. Timofte, V. De, and L. Van Gool, "Anchored neighborhood regression for fast example-based super-resolution," *IEEE Int. Conf. Comput. Vis. (ICCV)*, pp. 1920-1927, (2013)

[12] R. Timofte, V. De Smet, L. Van Gool, "A+: Adjusted anchored neighborhood regression for fast super-resolution," *Asian Conference on Computer Vision (ACCV)*, pp. 111-126, (2014)

[13] C. Dong, C. C. Loy, K. He and X. Tang, "Learning a deep convolutional network for image super-resolution," *Euro. Conf. Comput. Vis. (ECCV)*, pp. 184-199, (2014)

[14] Z. Cui, H. Chang, S. Shan, B. Zhong, and X. Chen, "Deep network cascade for image super-resolution," *Euro. Conf. Comput. Vis. (ECCV)*, pp. 49-64, (2014)

[15] N. Joshi, R. Szeliski, D.J. Kriegman, "PSF estimation using sharp edge prediction," *IEEE Conf. Computer Vision and Pattern Recognition (CVPR)*, pp. 1-8, (2008)

[16] T. Michaeli, M. Irani, "Nonparametric blind super-resolution," *IEEE Conf. Computer Vision (ICCV)*, pp. 945-952, (2013)

[17] T. Michaeli, M. Irani, "Blind deblurring using internal patch recurrence," European Conference on Computer Vision (ECCV), pp. 783-798, (2014)

[18] W. Shao, M. Elad, "Simple, accurate, and robust nonparametric blind super-resolution," *Lecture Notes in Computer Science*, 9219, pp. 333-348, (2015)

[19] W. Shao, H. Li, M. Elad, "Bi-L_0-L_2-norm regularization for blind motion deblurring," *Journal of Visual Communication and Image Representation*, 33, pp. 42-59, (2015)

[20] D. Krishnan, T. Tay, R. Fergus, "Blind deconvolution using a normalized sparsity measure," *IEEE Conf. Computer Vision and Pattern Recognition (CVPR)*, pp. 233-240, (2011)

[21] L. Xu, Q. Yan, Y. Xia, J. Jia, "Structure extraction from texture via relative total variation," *ACM Transactions on Graphics*, vol. 31, no. 6, article 139, (2012)

[22] A. Levin, Y. Weiss, F. Durand, W.T. Freeman, "Understanding blind deconvolution algorithms," *IEEE Trans. Pattern Analysis and Machine Intelligence*, vol. 33, no. 12, pp. 2354-2367, (2011)

[23] A. Marquina, S.J. Osher, "Image super-resolution by TV-regularization and Bregman iteration," *Journal of Scientific Computing*, 37: 367-382, (2008)